Journal of Materials Chemistry

Cite this: J. Mater. Chem., 2012, 22, 18908

www.rsc.org/materials

PAPER

N-Methyl-2-pyrrolidone-assisted solvothermal synthesis of nanosize orthorhombic lithium iron phosphate with improved Li-storage performance†

Xiaofei Liu,[a] Jia-Qi Huang,[b] Qiang Zhang,*[b] Xin-Yan Liu,[b] Hong-Jie Peng,[b] Wancheng Zhu*[a] and Fei Wei*[b]

Received 10th May 2012, Accepted 25th July 2012
DOI: 10.1039/c2jm32962j

Exploring an efficient and effective way for synthesis of lithium iron phosphate ($LiFePO_4$) with good Li-storage performance is a good way to fully demonstrate their applications for Li-ion batteries. In this contribution, $LiFePO_4$ nanoparticles were synthesized by a facile solvothermal process with water/*N*-methyl-2-pyrrolidone (NMP) solvent system at a moderate temperature of 180 °C. The product was determined as single-phase orthorhombic $LiFePO_4$, and the presence of crystal growth inhibitor NMP was favourable for the formation of smaller-sized $LiFePO_4$ particles with improved electrochemical properties. After a carbon coating process, the $LiFePO_4$/C sample afforded a reversible capacity of 140 mA h g^{-1} at 0.5 C, 106 mA h g^{-1} at 5.0 C at room temperature, and 163 mA h g^{-1} at 0.5 C, 153 mA h g^{-1} at 5.0 C at the higher temperature of 60 °C, respectively. The long cycle test at 0.2 C showed that no noticeable capacity fading was observed. The present $LiFePO_4$ obtained by the facile solvothermal process had good thermal and electrochemical stability, which were attributed to facile Li ion diffusion and a good electron transfer pathway in the solvothermal $LiFePO_4$ product.

1. Introduction

Lithium-ion rechargeable batteries are the most important power source for the increasing demand from portable electronic devices, electrical vehicles, hybrid electrical vehicles, *etc.* There has been a dramatic increase in research and commercialization activities of lithium-ion batteries for large scale energy storage and for on-board energy storage in electric vehicles and plug-in hybrid electric vehicles. Tremendous efforts have been devoted to explore alternatives to the toxic and expensive cobalt-oxide-based cathodes currently employed in commercialized lithium-ion batteries, particularly for potential use in large scale applications such as hybrid electric vehicles.[1,2] There is a great challenge in making low cost, high-performance, and high-safety lithium ion batteries for vehicle applications. Lithium iron phosphate ($LiFePO_4$), whose electrochemical activities were first reported by Padhi *et al.*,[3] is currently the subject of extensive studies as a cathode material for a new generation of Li-ion batteries. The main advantages of $LiFePO_4$ are its flat voltage profile, abundant raw material resources, low cost, low toxicity, remarkable thermal stability, and a relatively high theoretical specific capacity of 170 mA h g^{-1}.[4–6] In contrast, the drawbacks of $LiFePO_4$ include its poor electronic conductivity and low ionic diffusivity. Although the theoretical calculation showed that the intrinsic ionic diffusion coefficient is as high as 10^{-8} ($LiFePO_4$) to 10^{-7} ($FePO_4$) cm^2 s^{-1},[7] the one-dimensional (1D) channels are easily blocked by defects and impurities. The blockages in 1D paths are different from those in two-dimensional (2D) and three-dimensional (3D) paths where Li ions can move around the blocked sites.[5,8] The failure of 1D channel causes the slow kinetics of charging and discharging processes. To avoid the blockages of long channels, the construction of $LiFePO_4$ particles with certain morphologies is of high interest.[9,10] Nanosize pristine $LiFePO_4$ shows desirable electrochemical properties.[4,9–11] The introduction of a second component, such as a conductive carbon[12]/carbon nanotubes (CNTs)[13]/graphene[14] coating, doping with supervalent cations,[15] and surface modifications[16] by using a non-carbon second phase coating (*e.g.* metal oxides, polymers) have been well developed.

Up to now, both the solid state route (solid-state reaction, mechanochemical activation, carbothermal reduction, and microwave processing) and solution chemistry route (hydro/solvothermal processing, sol–gel process, precipitation, emulsion-drying and spray pyrolysis method) have been widely used for efficient synthesis of $LiFePO_4$.[17] The wet chemical preparation routes have an indisputable advantage over solid-state reactions in achieving better homogeneity and mixing of the starting compounds on the molecular level. A low temperature, soft chemistry route, such as hydro/solvothermal, is efficient, inexpensive, and sufficiently flexible so that the material's properties (*e.g.* cation distribution, particle size, and

[a]*Department of Chemical Engineering, Qufu Normal University, Shandong 273165, China. E-mail: zhuwancheng@tsinghua.org.cn*
[b]*Beijing Key Laboratory of Green Chemical Reaction Engineering and Technology, Department of Chemical Engineering, Tsinghua University, Beijing 100084, China. E-mail: zhang-qiang@mails.tsinghua.edu.cn; wf-dce@tsinghua.edu.cn*

† Electronic supplementary information (ESI) available: The data of rate performance, X-ray diffraction, and electrochemical impedance spectroscopy. See DOI: 10.1039/c2jm32962j

morphology) can be generally tailored by tuning the synthetic parameters.[18] For instance, Yang *et al.* reported a hydrothermal method for crystalline $LiFePO_4$ with a size of *ca.* 4 μm and an initial discharge capacity of 91 mA h g^{-1}.[19] $LiFePO_4$ synthesized by a hydrothermal process at 170 °C with a particle size of 0.5 μm exhibited a discharge capacity of 65 mA h g^{-1}.[20] Well-crystallized $LiFePO_4$ NPs,[21] $LiFePO_4$ microspheres with an average size of 0.5–1 (ref. 22) or ~3 μm (ref. 23) have been synthesized by a facile hydrothermal route. The size reduction strategy has been employed to improve the performance of $LiFePO_4$ during the hydro/solvothermal process. $LiFePO_4$ nanospheres with an average diameter of ~300 nm lodged in a 3D porous carbon structure were prepared by the mechanical ball milling activation of reactive precursors and a subsequent aging procedure in tanks.[24] $LiFePO_4$ hierarchical nanostructures self-assembled by nanoplates were successfully synthesized using polyvinylpyrrolidone (PVP) as the surfactant in a benzyl alcohol system.[25] Uniform $LiFePO_4$ nanoplates were obtained by a solvothermal method with ethylene glycol as the solvent.[10,26] The presence of ethylene glycol can unexpectedly induce the formation of gel-like intermediates, resulting in $LiFePO_4$ nanoparticles with a three-dimensional (3D) lattice structure.[27] It is highly expected that the Li-storage performance can be further improved if the role of the solvent and initial precursor for $LiFePO_4$ hydro/solvothermal growth can be well understood.

Herein, we report a solvothermal strategy for the synthesis of $LiFePO_4$ NPs in *N*-methyl-2-pyrrolidone (NMP) to provide new insights in the materials chemistry of $LiFePO_4$ synthesis and its energy storage properties. The reason for choosing NMP as the solvent is mainly due to its advantages in stability at ambient temperature, low volatility, low flammability, no clear toxicity profile, and its industrial scale usage in polymerization, petrochemical processing, surface coating and the plastics industry.[28] Assisted by NMP in the solvothermal synthesis and a further carbon coating process, small-sized $LiFePO_4$ NPs with an average diameter of *ca.* 100 nm with improved electrochemical Li-storage performance have been successfully acquired.

2. Experimental

2.1. Synthesis of $LiFePO_4$ NPs and $LiFePO_4$/C

$LiFePO_4$ NPs were synthesized by a facile solvothermal route with the molar ratio of $LiOH \cdot H_2O : FeSO_4 \cdot 7H_2O : H_3PO_4$ (85 wt%) = 3 : 1 : 1. All reagents were analytical grade and used as received without further purification. In a typical procedure, 0.02 mol $FeSO_4 \cdot 7H_2O$ was dissolved in 20 mL deionized (DI) water, and 0.02 mol H_3PO_4 was added to the above $FeSO_4$ solution. 0.06 mol $LiOH \cdot H_2O$ was dissolved in 24 mL DI water under magnetic stirring, and the resultant solution was slowly added to the former $FeSO_4$ solution, leading to a sticky gray white slurry. After that 50 mL NMP was added to the slurry under vigorous magnetic stirring for 20 min at room temperature, with the protection of N_2. Subsequently, the homogeneous slurry was transferred into a Teflon-lined stainless steel autoclave with a capacity of 200 mL, which was heated to 180 °C and kept in an isothermal state for 6.0 h. After the hydrothermal treatment, the autoclave was cooled down to room temperature naturally, and the as-synthesized gray white precipitate was filtered, washed with DI water three times, and finally vacuum dried at 80 °C for 24 h. To investigate the effect of NMP on the $LiFePO_4$ synthesis, $LiFePO_4$ was also prepared by a similar hydrothermal route using 50 mL of DI water as the sole solvent, with other conditions kept the same.

The carbon coating process for $LiFePO_4$/C was performed as follows: 4.0 g $LiFePO_4$ and 0.50 g glucose were added to a stainless steel shearer. After sufficient grinding, the mixtures were annealed within a tube furnace at 700 °C for 5 h under the mixed atmosphere of Ar and H_2 (volume ratio of $Ar : H_2 = 95 : 5$). After annealing, the as-obtained $LiFePO_4$ sample with carbon coating, *i.e.* $LiFePO_4$/C, was cooled down to room temperature naturally within the tube furnace and then collected for further characterization.

2.2. Electrochemical performance evaluation

To prepare the working cathode, a slurry was first made by mixing the $LiFePO_4$/C active material, CNTs, and polyvinylidene fluoride (PVDF) in NMP with a mass ratio of $LiFePO_4$/C : CNTs : PVDF = 80 : 15 : 5. The slurry was vigorously magnetically stirred for *ca.* 18 h, leading to a homogeneously mixed slurry, which was coated on an Al foil, and then dried in a vacuum drying oven at 120 °C for 12 h. Subsequently, the foil was punched into disks with a diameter of 13 mm for the working electrode. The electrochemical testing was carried out by coin cells of CR2025 with a Li foil as the anode, a microporous polyethylene sheet (Celgard 2400) as the separator, and $LiPF_6$ (1.0 M) as the electrolyte which was dissolved in a mixed solution of ethylene carbonate (EC)–dimethyl carbonate (DMC)–ethylene methyl carbonate (EMC) (mass ratio of EC : DMC : EMC = 1 : 1 : 1). The loading amount of $LiFePO_4$ electrodes is 1.30 and 1.46 mg cm^{-2} for hydro- and solvo-thermal samples, respectively. The carbon content is *ca.* 5 wt% in $LiFePO_4$/C NPs. All the assembly processes for the coin cells were conducted in an Ar-filled glove box. The cells were charged and discharged over a voltage range of 2.5–4.0 V at different currents. The cyclic voltammetry (CV) and electrochemical impedance spectroscopy (EIS) were carried out on a Solartron Analytical 1470E electrochemical workstation at a sweep rate of 0.1 mV s^{-1} between 2.5 and 4.0 V (*vs.* Li/Li^+). The specific discharge capacity of the battery was calculated based on the mass of pure $LiFePO_4$ in the working electrode.

2.3. Characterization

The structure of the sample was identified by an X-ray powder diffractometer (XRD, D8-Advance, Bruker, Germany) using Cu K_α radiation ($\lambda = 1.54178$ Å) and a fixed power source (40.0 kV, 40.0 mA). The morphology and microstructure of the samples were examined by field emission scanning electron microscopy (SEM, JSM 7401F, JEOL, Japan) and high resolution transmission electron microscopy (TEM, JEM-2010, JEOL, Japan). Brunauer–Emmett–Teller (BET) surface area measurements were conducted in a Quadarasorb SI automated surface area and porosity analyzer with N_2 as the adsorption gas.

3. Results and discussion

3.1. The pristine hydro-/solvo-thermal $LiFePO_4$ nanoparticles

Fig. 1 shows the composition and morphology of the products obtained by the hydro- (Fig. 1(a_1 and b)) and solvo-thermal (Fig. 1(a_2 and c)) processes. The XRD patterns showed that both the hydro- (Fig. 1(a_1)) and solvo-thermal (Fig. 1(a_2)) products were composed of pure phase, orthorhombic olivine $LiFePO_4$ (JCPDS no. 83-2092). No distinct diffraction peaks of other impurities were detected, indicating the high purity of the products. The obtained lattice parameters for the hydro- and solvo-thermal $LiFePO_4$ are $a = 10.2838$ Å, $b = 5.9562$ Å, $c = 4.6459$ Å, and $a = 10.2323$ Å, $b = 5.9353$, $c = 4.6609$, respectively. These values are comparable with reported values in the literature.[10] The BET surface area of the hydro- and solvo-thermal $LiFePO_4$ NPs were 4.5 and 11.8 $m^2\ g^{-1}$, respectively. In addition, compared with that of the hydrothermal product, the X-ray diffraction peaks of the as-obtained solvothermal product exhibited a broadening characteristic, revealing that the introduction of NMP promoted the formation of $LiFePO_4$ NPs with a smaller size, which is the key factor for a high-performance electrode material.[1,4,5,29]

As shown in Fig. 1(b), the hydrothermal product particles synthesized in the absence of NMP were mainly composed of irregular quasi-hexagonal or rhombic plates. From the size distribution shown as the inset of Fig. 1(b), the $LiFePO_4$ particles had a length of 0.3–1.0 μm, a width of 0.15–0.7 μm, and a thickness of 0.1–0.2 μm. In comparison, the solvothermal product particles obtained in the presence of NMP consisted of relatively uniform NPs (Fig. 1(c and d)). As illustrated in the inset of Fig. 1(d), the solvothermal $LiFePO_4$ NPs are much smaller than the hydrothermal products. Obviously, the introduction of the solvent NMP favored the formation of smaller particles of $LiFePO_4$ (Fig. 1(c and d)), in accordance with the XRD results (Fig. 1(a_1 and a_2)). The $LiFePO_4$ crystal growth mechanism during the solvothermal reaction was deemed to consist of the dissolution of the precursor and nucleation, growth and aggregation, partial dissolution, and complete crystallization.[30] As a strong polar organic solvent, the activated NMP obtained by boiling purified NMP with H_2O and O_2 is an effective reducing agent that allows rapid reduction of metal ions. During the solvothermal growth of $LiFePO_4$, the polar NMP molecules are assumed to be a weak reducing agent that prevents the oxidation of Fe^{2+} to Fe^{3+} during the $LiFePO_4$ growth and helps ensure the purity of the products. The NMP affords a much higher viscosity than common solvents such as water and ethanol, therefore, the ion diffusion rate was slowed down and large particle growth was prevented. Therefore, the NMP can not only act as a solvent, but also as a crystal growth inhibitor of $LiFePO_4$. Ag nanoparticles[31] and ferrite nanocrystals[28] have been available when NMP has been used as the solvent in previous publications. Herein the nanosized $LiFePO_4$ particles are expected to have a short diffusion length for Li^+ diffusion during the charge–discharge process. This is well confirmed by the rate performance shown in Fig. S1(a).† The solvothermal $LiFePO_4$ particles render a reversible capacity of

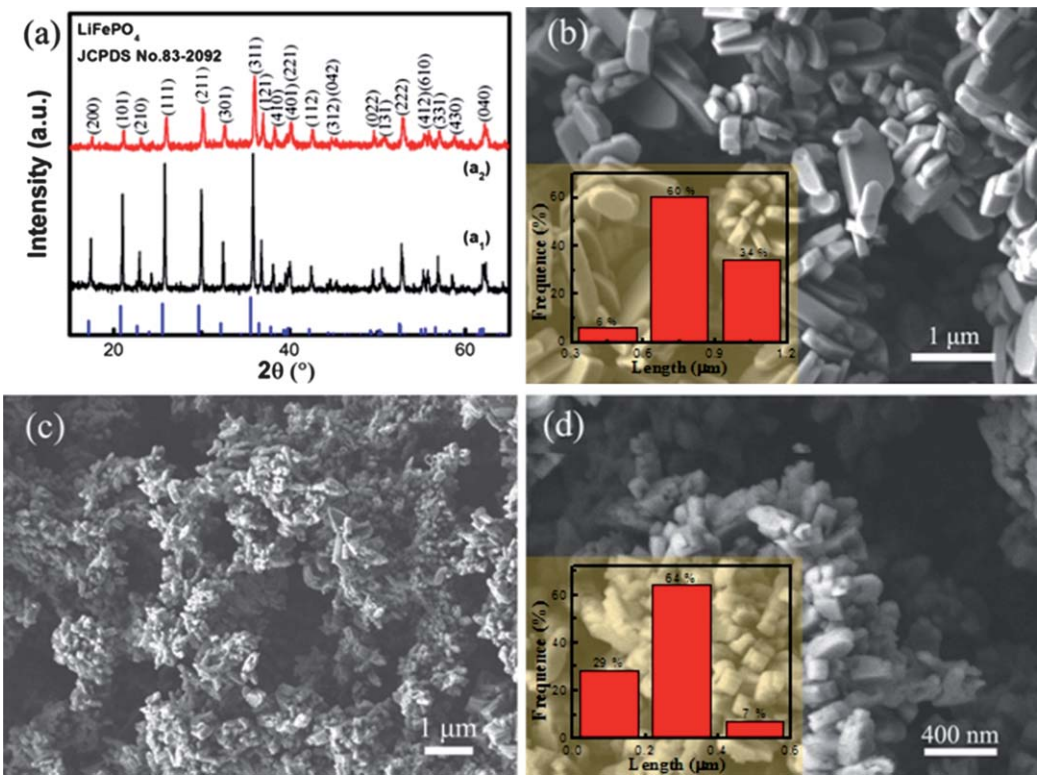

Fig. 1 (a) XRD patterns and (b, c and d) SEM images of the (a_1 and b) hydrothermal and (a_2, c and d) solvothermal $LiFePO_4$ synthesized at 180 °C for 6.0 h, with the molar ratio of $Li^+ : Fe^{2+} : PO_4^{3-} = 3 : 1 : 1$. The vertical lines in the XRD patterns are the standard pattern of orthorhombic $LiFePO_4$. The insets in (b) and (d) are the length distributions of the $LiFePO_4$ NPs.

82 mA h g^{-1} at a current rate of 0.2 C, while that of hydrothermal $LiFePO_4$ is only 75 mA h g^{-1}. After annealing at 700 °C, the crystallization of the $LiFePO_4$ samples improved, and the defect density decreased. As a result, the Li-ion diffusion through the 1D channel became easy. The capacities of hydro- and solvothermal samples rise to 94 and 110 mA h g^{-1} after annealing, respectively (Fig. S1(b)†). The smaller NPs of solvothermal $LiFePO_4$ exhibit a higher discharge capacity than the large $LiFePO_4$ obtained by hydrothermal synthesis. Nanosize particles with a short Li^+ diffusion length are promising advanced electrode materials. However, the capacity of carbon-free $LiFePO_4$ is still low, which can be attributed to its poor electrical conductivity and the limited utilization of the cathode materials.

3.2. Carbon coating of the $LiFePO_4$ nanoparticles

The most effective way to increase conductivity is to apply a carbon coating on the $LiFePO_4$ particles surface. The carbon particles play the role of forming a conductive network in the cathode coating to improve surface electronic conductivity of $LiFePO_4$ particles and decrease the polarization resistance of the electrode, helping to obtain the best rate performance. Furthermore, the additional carbon source is a driving force for the formation of small particles, which are covered with a few nanometers-thick carbon coating.[5,32,33] The morphologies and structures of the $LiFePO_4$/C particles are shown in Fig. 2 and S2.† After hydro-/solvo-thermal reaction and heat treatment at 700 °C for 5 h using glucose as carbon source, the $LiFePO_4$ agglomerates dispersed into separated particles during the carbon coating process. The structure of $LiFePO_4$ was well preserved after annealing and carbon coating (Fig. S2†). Some small pores were observed, which was anticipated to be helpful for electrolyte penetration.[34] Compared with $LiFePO_4$/C particles obtained by the hydrothermal process (Fig. 2(a and c)), the size of $LiFePO_4$/C particles through solvothermal process was much smaller (Fig. 2(b and e)). The solvothermal $LiFePO_4$ NPs were with a length of *ca.* 100–200 nm (inset in Fig. 2(b)). A 2.5 or 2.3 nm-thick carbon layer was observed on the surface of the two samples, respectively (Fig. 2(d and f)). The $LiFePO_4$ NPs derived from hydro- or solvo-thermal processes also displayed homogeneous lattice fringes in high resolution TEM images with a spacing of 0.299 or 0.296 nm, which were assigned to the (211) crystal plane of the orthorhombic $LiFePO_4$. The BET surface area of the hydro- and solvo-thermal $LiFePO_4$/C were 10.5 and 24.9 m^2 g^{-1}, respectively.

3.3. Electrochemical performance of $LiFePO_4$ from solvothermal route

In order to explore the potential applications of $LiFePO_4$ in high-power Li-ion batteries, the electrochemical properties of $LiFePO_4$ and $LiFePO_4$/C samples were evaluated with 2025-type coin half-cells at both 25 and 60 °C. CV was performed for both the hydro- and solvo-thermal samples, with the operation voltage in the range 2.5 to 4.0 V *vs.* Li/Li^+. Fig. 3(a and b) show the first three cycles of the CV profiles of both samples at a scanning rate of 0.1 mV s^{-1}. The electrodes of both samples show a couple of anodic and cathodic peaks in the range of 3.26 to 3.60 V, corresponding to the two-phase charge/discharge reaction between $LiFePO_4$ and $FePO_4$. The positions of redox peaks correspond to the extraction and insertion of Li^+.[5,33] During the first cycle of hydrothermal NP electrodes, the anodic peak is at 3.7 V, the corresponding cathodic peak is at 3.3 V. In the second and third cycles, the anodic peak is at 3.58 V, and the corresponding cathodic peak is unaltered. The anodic and cathodic peaks are at 3.58 and 3.33 V, respectively, for the solvothermal electrodes during the first cycle. In the subsequent two cycles, both the anodic and cathodic peak intensities increase. The solvothermal $LiFePO_4$/C cathode material with a smaller size distribution affords approximately symmetrical peaks, indicating the better insertion/extraction reversibility than that of the hydrothermal sample.

Fig. 4(a) shows the first and second charge–discharge curves of the hydro/solvothermal $LiFePO_4$/C samples at 0.2 C. The solvothermal $LiFePO_4$/C composite exhibits a discharge capacity of 147 mA h g^{-1}, while that of the hydrothermal $LiFePO_4$/C is 118 mA h g^{-1}. Moreover, both the solvothermal and hydrothermal samples demonstrate a flat plateau around 3.4 V, while the voltage plateau for solvothermal $LiFePO_4$/C NPs shows a lower degree of polarization and also a longer voltage plateau. The superior Li storage performance is attributed to the excellent electronic conductivity and ionic diffusivity of $LiFePO_4$ nanoparticles derived from the $LiFePO_4$ NPs and the uniform carbon coating.

As with the requirement for electric vehicle applications, rate performance and thermal stability are also key factors for lithium-ion battery cathode materials.[4,5,35] The $LiFePO_4$/C from the hydrothermal process exhibits a reversible discharge capacity of 122 or 79 mA h g^{-1} at a charge–discharge current of 0.2 C or 5.0 C (red line, filled symbols, Fig. 4(b)) at room temperature. In contrast, the $LiFePO_4$/C from the solvothermal process has reversible capacities of 150, 140, and 106 mA h g^{-1} at a rate of 0.2, 0.5, and 5.0 C, respectively (black line, filled symbols, Fig. 4(b)). Although the specific capacity gradually decreases with increasing current rate, a high capacity still remains at 5.0 C. This indicates that the solvothermal $LiFePO_4$/C can endure high rate charge and discharge. The current Li storage performance affords a significantly improved Li-storage performance than the early $LiFePO_4$ product by hydrothermal process (a discharge capacity of 91 mA h g^{-1} at 0.14 mA cm^{-2} (ref. 19) or 65 mA h g^{-1} at 0.1 C (ref. 20)), and is competitive to recent progress of $LiFePO_4$/C nanocomposites, such as the core–shell $LiFePO_4$@C composites with a discharge capacity of 138 mA h g^{-1} at 0.1 C,[36] olivine-type $LiFePO_4$ using dimethyl sulfoxide as a boiling point raiser and crystal growth inhibitor with a discharge capacity of 157.7 mA h g^{-1} at 0.2 C,[37] and hierarchically porous $LiFePO_4$/C nanocomposites with a discharge capacity of 140 mA h g^{-1} at 0.1 C.[38] In the present work, the solvothermal $LiFePO_4$ affords an improved Li storage performance, especially at high current rate, which is speculated to be due to the small size and facile Li ion diffusion. The carbon outer layer provides an efficient electron pathway. This is similar to the reports by Qin *et al.*[35] They found that $LiFePO_4$ obtained by hydrothermal growth affords a discharge capacity of 128 mA h g^{-1} at 0.5 C, while an improved capacity of 160 mA h g^{-1} at 0.5 C was presented for $LiFePO_4$ nanoparticles prepared with ethylene glycol (EG) as solvent and template.[35] The obvious improvement is attributed to simultaneous suppression of crystal growth and defect concentration reduction of the FeLi antisite during solvothermal synthesis in EG solution.

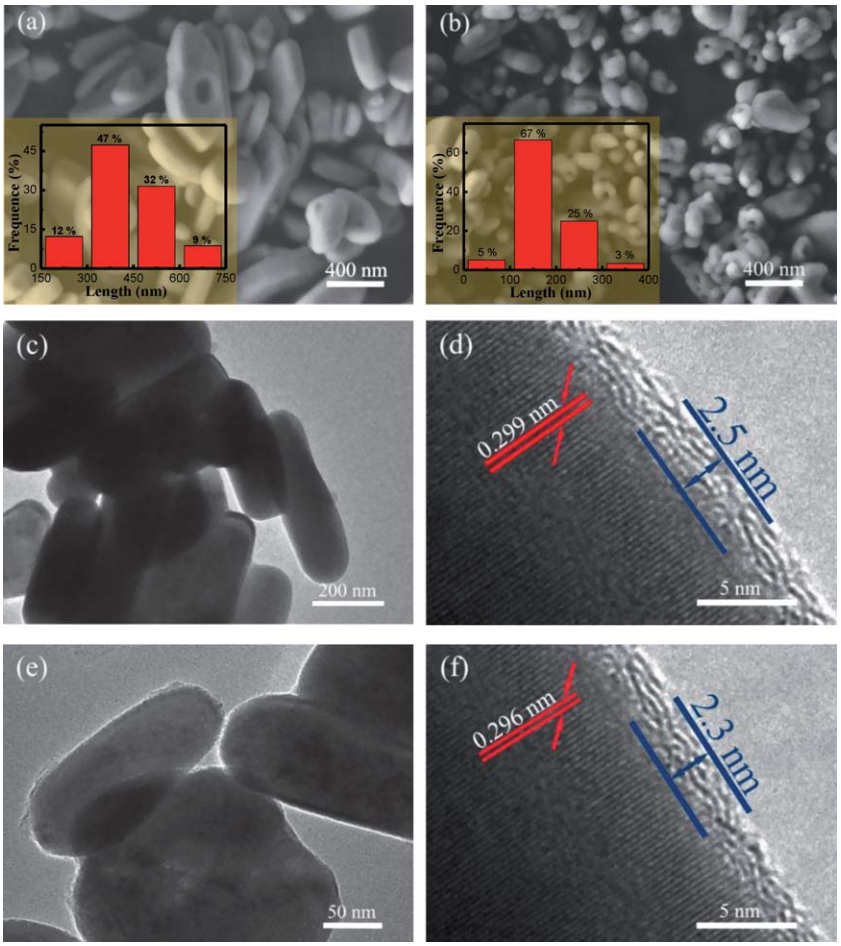

Fig. 2 SEM images of (a) hydrothermal and (b) solvothermal $LiFePO_4$/C NPs; TEM and high resolution TEM images of (c and d) hydrothermal and (e and f) solvothermal $LiFePO_4$/C nanoparticles. The insets in (a) and (b) are the length distributions of the $LiFePO_4$/C NPs. Annealing conditions: temperature: 700 °C, time: 5 h, weight ratio: $LiFePO_4$: glucose = 8 : 1.

The Li-ion storage capability of the $LiFePO_4$ electrode is greatly affected by the operation temperature. Fig. 4(c) shows the high temperature performances of the two samples. Both samples were tested at 60 °C at various charge and discharge currents. When the operation temperature increased, the Li^+ diffusion was enhanced. As a result, the charge and discharge capacities of hydro- and solvo-thermal $LiFePO_4$/C NPs were increased obviously compared with the results obtained at 25 °C, especially for the $LiFePO_4$ nanoparticles obtained by solvothermal process. With the increasing of charge–discharge current densities, the Columbic efficiency was boosted to around 100% (5.0 C). The typical solvothermal sample shows specific capacities of 163, 159, and 153 mA h g^{-1} at currents of 0.5, 2.0, and 5.0 C, respectively. Both samples exhibit excellent thermal and electrochemical stability, suggesting that the olivine type structure of the samples has been maintained even at high rate charge and discharge. This is similar to the reports by Kurita *et al.*,[39] in which the discharge capacity of $LiFePO_4$ enhanced with increasing temperature

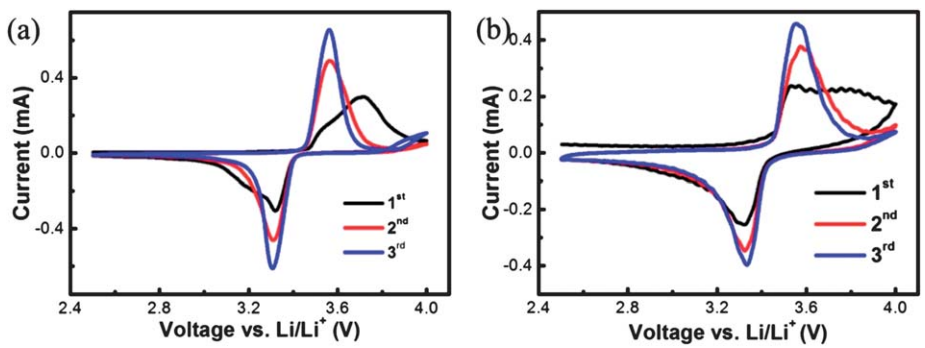

Fig. 3 The representative CV profiles of the (a) hydrothermal and (b) solvothermal $LiFePO_4$/C samples at a scan rate of 0.1 mV s^{-1}.

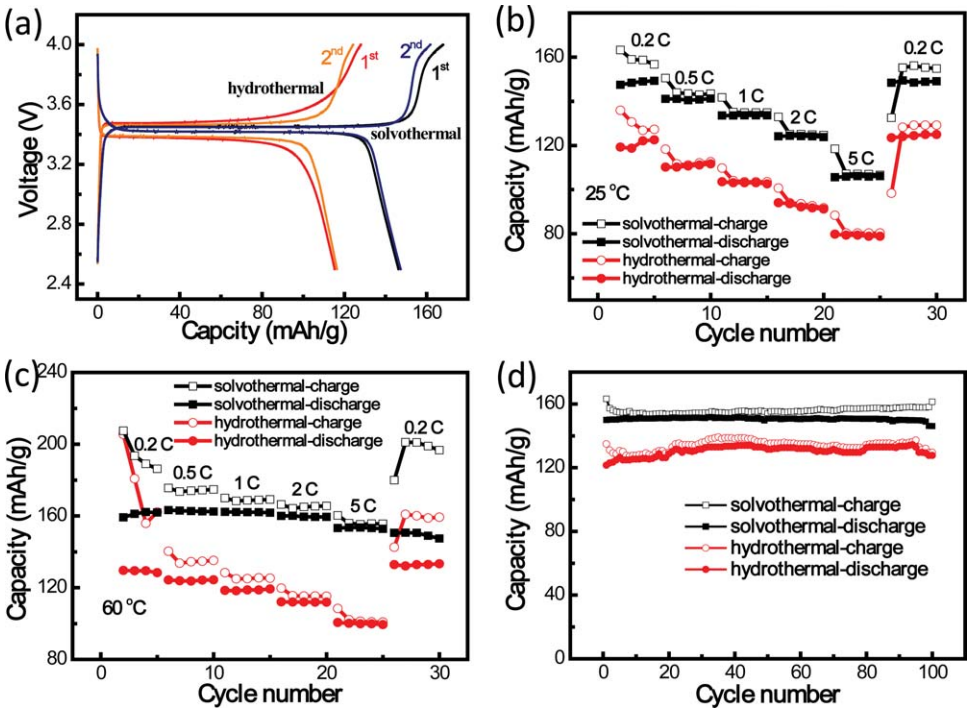

Fig. 4 (a) The first and second charge–discharge curves of the hydrothermal and solvothermal $LiFePO_4$/C NPs at a current of 0.2 C (1 C = 170 mA g^{-1}, a rate of *n* C corresponds to the full discharge in 1/*n* h); the rate performance (charge–discharge capacity) of the hydrothermal and solvothermal $LiFePO_4$/C NPs at (b) 25 °C and (c) 60 °C; (d) the cycling performance (charge–discharge capacity) of the hydrothermal and solvothermal $LiFePO_4$/C NPs at a current of 0.2 C. Filled symbols: charge capacity; open symbols: discharge capacity.

below 100 °C. Such significant improvement of the thermal performance is attributed to enhancement of the reaction speed of $LiFePO_4$ electrode and an improved lithium-ion conductivity following the Arrhenius equation.

The cycling performance of both samples at 0.2 C was also investigated. Both electrodes from hydro- and solvo-thermal processes show a stable cycling performance (Fig. 4(d)). The test cells were with a capacity degradation of less than 3.0% after 100 cycles. After 100 cycles, the test cell of the solvothermal sample still delivered a specific capacity of 150 mA h g^{-1}, demonstrating a stable cycling performance at a low current rate for $LiFePO_4$/C nanocomposites.

Electrochemical impedance spectroscopy was used to understand the electrode kinetics and evaluate electrode impedance of the hydrothermal and solvothermal $LiFePO_4$/C cathodes. The impedance spectra were measured with Li-metal as the counter electrode at various voltages (2.5–4.0 V) during the first charge–discharge cycle. Fig. S3† shows the Nyquist plots for the two samples. During both charge–discharge cycles a single semicircle can be observed and the fitting equivalent circuit is shown in Fig. S4,†[40] in which R_s is associated with the solution resistance of electrolyte, R_f and CPE1 are related to the solid-state diffusion of Li^+ through the solid electrolyte interface and its corresponding constant phase element (CPE), R_{ct} and CPE2 signify the charge transfer resistance and the corresponding CPE. W_o is the Warburg impedance element attributable to the diffusion of lithium ions in the active materials, C_i is the intercalation capacitance. The fitting results are listed in Table S1.† The resistance values of both hydro- and solvo-thermal $LiFePO_4$/C NPs electrodes during the charge–discharge cycles show a similar trend, however, the $R_{(f+ct)}$ values at various voltages of solvothermal $LiFePO_4$/C NPs are smaller than those of the hydrothermal $LiFePO_4$/C NPs. Such fitting results provided unambiguous evidence for the easy and fast Li ion diffusion and good electron transfer pathway of the solvothermal products. Such improved kinetics for the solvothermal $LiFePO_4$/C electrode benefit from the smaller size of the NPs, which has been confirmed by the XRD patterns, SEM and TEM images (Fig. 1 and 2).

4. Conclusions

Single-phase orthorhombic $LiFePO_4$ NPs were synthesized by a facile solvothermal process with a water/NMP solvent system at a moderate temperature of 180 °C. The presence of NMP is speculated to be an effective reducing agent and crystal growth inhibitor, therefore, the as-obtained $LiFePO_4$ NPs had a reduced size. After a carbon coating process, the $LiFePO_4$/C sample showed a reversible capacity of 140 mA h g^{-1} at 0.5 C, 106 mA h g^{-1} at 5.0 C at room temperature, and 163 mA h g^{-1} at 0.5 C, 153 mA h g^{-1} at 5.0 C at elevated temperature (60 °C). During a long cycle test at 0.2 C, the discharge capacity showed no noticeable fading. The electrochemical performance was superior to $LiFePO_4$ nanoparticles from a hydrothermal process. Such excellent electrochemical performance was attributed to the easy and fast Li ion diffusion and good electron transfer pathway in the solvothermal products. This provided a facile chemical way to obtain a $LiFePO_4$/C nanocomposite with excellent Li storage performance for board applications in hybrid electrical vehicles and plug-in hybrid electric vehicles.

Acknowledgements

This work was supported by the National Basic Research Program of China (973 Program, 2011CB932602), Project of Shandong Province Higher Educational Science and Technology Program, China (J10LB15), the Excellent Middle-Aged and Young Scientist Award Foundation of Shandong Province, China (BS2010CL024), and the China Postdoctoral Science Foundation (2011M500022).

Notes and references

1 J. M. Tarascon, N. Recham, M. Armand, J. N. Chotard, P. Barpanda, W. Walker and L. Dupont, *Chem. Mater.*, 2010, **22**, 724.
2 H. Li, Z. X. Wang, L. Q. Chen and X. J. Huang, *Adv. Mater.*, 2009, **21**, 4593; J. W. Fergus, *J. Power Sources*, 2010, **195**, 939; C. Liu, F. Li, L. P. Ma and H. M. Cheng, *Adv. Mater.*, 2010, **22**, E28; D. S. Su and R. Schlogl, *ChemSusChem*, 2010, **3**, 136.
3 A. K. Padhi, K. S. Nanjundaswamy and J. B. Goodenough, *J. Electrochem. Soc.*, 1997, **144**, 1188.
4 W. J. Zhang, *J. Power Sources*, 2011, **196**, 2962.
5 J. J. Wang and X. L. Sun, *Energy Environ. Sci.*, 2012, **5**, 5163.
6 L. X. Yuan, Z. H. Wang, W. X. Zhang, X. L. Hu, J. T. Chen, Y. H. Huang and J. B. Goodenough, *Energy Environ. Sci.*, 2011, **4**, 269; Y. G. Wang, P. He and H. S. Zhou, *Energy Environ. Sci.*, 2011, **4**, 805; W. J. Zhang, *J. Electrochem. Soc.*, 2010, **157**, A1040.
7 D. Morgan, A. Van der Ven and G. Ceder, *Electrochem. Solid-State Lett.*, 2004, **7**, A30.
8 H. S. Fang, Z. Y. Pan, L. P. Li, Y. Yang, G. F. Yan, G. S. Li and S. Q. Wei, *Electrochem. Commun.*, 2008, **10**, 1071.
9 P. Balaya, *Energy Environ. Sci.*, 2008, **1**, 645.
10 K. Saravanan, M. V. Reddy, P. Balaya, H. Gong, B. V. R. Chowdari and J. J. Vittal, *J. Mater. Chem.*, 2009, **19**, 605; K. Saravanan, P. Balaya, M. V. Reddy, B. V. R. Chowdari and J. J. Vittal, *Energy Environ. Sci.*, 2010, **3**, 457.
11 P. G. Bruce, B. Scrosati and J. M. Tarascon, *Angew. Chem., Int. Ed.*, 2008, **47**, 2930.
12 F. Croce, A. D. Epifanio, J. Hassoun, A. Deptula, T. Olczac and B. Scrosati, *Electrochem. Solid-State Lett.*, 2002, **5**, A47; J. J. Chen and M. S. Whittingham, *Electrochem. Commun.*, 2006, **8**, 855; C. B. Zhu, Y. Yu, L. Gu, K. Weichert and J. Maier, *Angew. Chem., Int. Ed.*, 2011, **50**, 6278.
13 X. L. Li, F. Y. Kang, X. D. Bai and W. Shen, *Electrochem. Commun.*, 2007, **9**, 663.
14 F. Y. Su, C. H. You, Y. B. He, W. Lv, W. Cui, F. M. Jin, B. H. Li, Q. H. Yang and F. Y. Kang, *J. Mater. Chem.*, 2010, **20**, 9644.
15 J. Ma, B. H. Li, H. D. Du, C. J. Xu and F. Y. Kang, *Electrochim. Acta*, 2011, **56**, 7385; J. Ma, B. H. Li, H. D. Du, C. J. Xu and F. Y. Kang, *J. Electrochem. Soc.*, 2011, **158**, A26.
16 B. Kang and G. Ceder, *Nature*, 2009, **458**, 190; Y. Jin, C. P. Yang, X. H. Rui, T. Cheng and C. H. Chen, *J. Power Sources*, 2011, **196**, 5623.
17 D. Jugovic and D. Uskokovic, *J. Power Sources*, 2009, **190**, 538.
18 M. K. Devaraju and I. Honma, *Adv. Energy Mater.*, 2012, **2**, 284.
19 S. F. Yang, P. Y. Zavalij and M. S. Whittingham, *Electrochem. Commun.*, 2001, **3**, 505.
20 K. Dokko, K. Shiraishi and K. Kanamuraa, *J. Electrochem. Soc.*, 2005, **152**, A2199.
21 J. F. Ni, M. Morishita, Y. Kawabe, M. Watada, N. Takeichi and T. Sakai, *J. Power Sources*, 2010, **195**, 2877.
22 Z. L. Wang, S. R. Su, C. Y. Yu, Y. Chen and D. G. Xia, *J. Power Sources*, 2008, **184**, 633.
23 J. F. Qian, M. Zhou, Y. L. Cao, X. P. Ai and H. X. Yang, *J. Phys. Chem. C*, 2010, **114**, 3477.
24 J. Q. Zhao, J. P. He, J. H. Zhou, Y. X. Guo, T. Wang, S. C. Wu, X. C. Ding, R. M. Huang and H. R. Xue, *J. Phys. Chem. C*, 2011, **115**, 2888.
25 H. Yang, X. L. Wu, M. H. Cao and Y. G. Guo, *J. Phys. Chem. C*, 2009, **113**, 3345.
26 M. Wu, Z. H. Wang, L. X. Yuan, W. X. Zhang, X. L. Hu and Y. H. Huang, *Chin. Sci. Bull.*, 2012, DOI: 10.1007/s11434-012-5019-0; C. Y. Nan, J. Lu, C. Chen, Q. Peng and Y. D. Li, *J. Mater. Chem.*, 2011, **21**, 9994.
27 W. P. Kang, C. H. Zhao, R. Liu, F. F. Xu and Q. Shen, *CrystEngComm*, 2012, **14**, 2245.
28 S. Verma and D. Pravarthana, *Langmuir*, 2011, **27**, 13189.
29 A. Manthiram, A. V. Murugan, A. Sarkar and T. Muraliganth, *Energy Environ. Sci.*, 2008, **1**, 621.
30 J. Lim, J. Gim, S. W. Kang, S. Baek, H. Jeong and J. Kim, *J. Electrochem. Soc.*, 2012, **159**, A479.
31 S. H. Jeon, P. Xu, N. H. Mack, L. Y. Chiang, L. Brown and H. L. Wang, *J. Phys. Chem. C*, 2010, **114**, 36.
32 Z. H. Chen and J. R. Dahn, *J. Electrochem. Soc.*, 2002, **149**, A1184; C. Su, X. D. Bu, L. H. Xu, J. L. Liu and C. Zhang, *Electrochim. Acta*, 2012, **64**, 190; S. Yoon, C. Liao, X. G. Sun, C. A. Bridges, R. R. Unocic, J. Nanda, S. Dai and M. P. Paranthaman, *J. Mater. Chem.*, 2012, **22**, 4611.
33 W. P. Kang, F. L. Liu, Y. L. Su, D. J. Wang and Q. Shen, *CrystEngComm*, 2011, **13**, 4174.
34 G. X. Wang, H. Liu, J. Liu, S. Z. Qiao, G. Q. M. Lu, P. Munroe and H. Ahn, *Adv. Mater.*, 2010, **22**, 4944.
35 X. Qin, J. M. Wang, J. Xie, F. Z. Li, L. Wen and X. H. Wang, *Phys. Chem. Chem. Phys.*, 2012, **14**, 2669.
36 B. Zhao, Y. Jiang, H. J. Zhang, H. H. Tao, M. Y. Zhong and Z. Jiao, *J. Power Sources*, 2009, **189**, 462.
37 Z. R. Chang, H. W. Tang, Y. Liu, X. Z. Yuan, H. J. Wang and S. Y. Gao, *J. Electrochem. Soc.*, 2012, **159**, A331.
38 C. M. Doherty, R. A. Caruso, B. M. Smarsly, P. Adelhelm and C. J. Drummond, *Chem. Mater.*, 2009, **21**, 5300.
39 T. Kurita, J. C. Lu, M. Yaegashi, Y. Yamada, S.-I. Nishimura, T. Tanaka, T. Uzumaki and A. Yamada, *J. Power Sources*, 2012, **214**, 166.
40 M. V. Reddy, G. V. S. Rao and B. V. R. Chowdari, *J. Phys. Chem. C*, 2007, **111**, 11712; M. V. Reddy, G. V. S. Rao and B. V. R. Chowdari, *J. Power Sources*, 2010, **195**, 5768; A. Sakunthala, M. V. Reddy, S. Selvasekarapandian, B. V. R. Chowdari and P. C. Selvin, *J. Phys. Chem. C*, 2010, **114**, 8099; M. V. Reddy, G. V. Subba Rao and B. V. R. Chowdari., *J. Mater. Chem.*, 2011, **21**, 10003.